



Adsorption effectiveness of β -lactoglobulin onto gold surface determined by quartz crystal microbalance

B. Jachimska^{a,*}, S. Świątek^a, J.I. Loch^b, K. Lewiński^b, T. Luxbacher^c

^a Jerzy Haber Institute of Catalysis and Surface Chemistry, PAS, Niezapominajek 8, 30-239 Cracow, Poland

^b Jagiellonian University, Faculty of Chemistry, Department of Crystal Chemistry and Crystal Physics, Biocrystallography Group, Ingardena 3, 30-060 Cracow, Poland

^c Anton Paar GmbH, Anton-Paar-Strasse 20, 8045 Graz, Austria

ARTICLE INFO

Article history:

Received 19 November 2017

Received in revised form 20 December 2017

Accepted 22 January 2018

Available online 31 January 2018

Keywords:

LGB adsorption

Zeta potential of gold surface

Quartz crystal microbalance with dissipation

Dynamic light scattering

Electrophoretic mobility

ABSTRACT

Bovine β -lactoglobulin (LGB) is a transport protein that can bind to its structure hydrophobic bioactive molecules. Due to the lack of toxicity, high stability and pH-dependent molecular binding mechanism, lactoglobulin can be used as a carrier of sparingly soluble drugs. Dynamic light scattering has confirmed LGB's tendency to create oligomeric forms. The hydrodynamic diameter of LGB molecules varies from 4 nm to 6 nm in the pH range of 2–10 and ionic strength $I = 0.001$ – 0.15 M, which corresponds to the presence of mono or dimeric LGB forms. The LGB zeta potential varies from 26.5 mV to -33.3 mV for $I = 0.01$ M and from 13.3 mV to -16 mV for $I = 0.15$ M in the pH range of 2–10. The isoelectric point is at pH 4.8. As a result of strong surface charge compensation, the maximum effective ionization degree of the LGB molecule is 35% for ionic strength $I = 0.01$ M and 22% for $I = 0.15$ M. The effectiveness of adsorption is linked with the properties of the protein, as well as those of the adsorption surface. The functionalization of gold surfaces with β -lactoglobulin (LGB) was studied using a quartz crystal microbalance with energy dissipation monitoring (QCM-D). The effectiveness of LGB adsorption correlates strongly with a charge of gold surface and the zeta potential of the molecule. The greatest value of the adsorbed mass was observed in the pH range in which LGB has a positive zeta potential values, below pH 4.8. This observation shows that electrostatic interactions play a dominant role in LGB adsorption on gold surfaces. Based on the adsorbed mass, protein orientation on gold surfaces was determined. The preferential side-on orientation of LGB molecules observed in the adsorption layer is consistent with the direction of the molecule dipole momentum determined by molecular dynamics simulations of the protein (MD). The use of the QCM-D method also allowed us to determine the effectiveness of adsorption of LGB on gold surface. Knowing the mechanism of LGB adsorption is significant importance for determining the optimum conditions for immobilizing this protein on solid surfaces. As β -lactoglobulin is a protein that binds various ligands, the binding properties of immobilized β -lactoglobulin can be used to design controlled protein structures for biomedical applications.

© 2018 Elsevier B.V. All rights reserved.

1. Introduction

β -Lactoglobulin (LGB), which belongs to the lipocalin superfamily, is the major whey protein in cow's milk. Under physiological conditions (pH 7 and concentration $> 50 \mu\text{M}$) LGB is predominantly dimeric [1,2]. Self-association of LGB to form larger oligomers has been reported in the pH range 3.7–5.2 with a maximum at approximately pH 4.6, just below the isoelectric point [2,3]. The oligomerization is more pronounced for isoform A than for isoform B indicating the involvement of specific interactions in this process [3]. The biological function of LGB is still unclear. It can bind to physiologically relevant ligands such as steroids, fatty acids, retinoids, vitamin D, cholesterol and local anesthetics [4–7]. Despite of many investigations of LGB, adsorption on

different surfaces, such as stainless steel [8], chromium [9,10], silicon [11], silica substances [12], polysulfone and polystyrene [13,14], the mode of the mechanism of its adsorption on a solid surface, especially on metals, remains to be clarified [15]. Understanding the adsorption behavior of LGB on metal surfaces is essential for the reduction of bio-fouling, a problem observed during food and drug production. Analysis of the experimental data shows that there are still inconsistent opinions about the mechanism of β -lactoglobulin protein adsorption concerning adsorption kinetics, structural reorientation or conformation, and protein aggregation whether in a solution or on the surface [16,17].

The properties of the adsorbed protein layer are highly dependent on the shape, effective charge and structure of the protein as these factors influence surface affinity, surface coverage, and hydration of the layer. The reversibility of the protein adsorption process depends on the polarity, hydrophobicity and surface roughness. Also, in the case of proteins, a preferential interaction with the surface is observed, a

* Corresponding author.

E-mail address: ncjachim@cyf-kr.edu.pl (B. Jachimska).

consequence of occurrence of the heterogeneous surface of the protein molecule. The development of new analytical techniques makes it possible to study protein adsorption with increasing accuracy [14,18–21]. Techniques such as quartz crystal microbalance (QCM), or surface plasmon resonance (SPR) enable a highly sensitive, qualitative, realtime, label-free, and noninvasive detection of adsorbed macromolecules.

In this work, we determined several basic physicochemical properties of LGB, including the diffusion coefficient (expressed as hydrodynamic diameter), electrophoretic mobility, which made it possible to determine the isoelectric point, and the non-compensated charge of the LGB molecule. As a substrate for adsorption, we chose gold owing to the fact that this metal is an attractive surface for many biological and medical applications, mostly due to its chemical stability and biocompatibility. Also, the number of investigations concerning the use of a gold surface in modern science is constantly increasing. In our previous work, by using a wide range of methods, we demonstrated that the conditions under which the adsorption occurred had a significant influence on the structure and properties of the adsorbed protein layer [22–24]. To qualitatively describe the LGB adsorption process on the surface of gold, we have determined the zeta potential of gold using the streaming potential method. The high sensitive technique of a quartz crystal microbalance with dissipation monitoring (QCM-D) allows us to determine the adsorbed amount and the visco-elastic properties of the adsorbed layer. Experimental data obtained from the QCM-D measurements were analyzed using the Sauerbrey based model to acquire quantitative information about viscoelastic properties of the protein layers formed on gold surfaces. These investigations lead to a more profound understanding of the self-assembling behavior of LGB layers, which are interesting candidates for drug delivery systems.

2. Materials and methods

2.1. Materials

A mixture of isoforms A and B of bovine β -lactoglobulin ($\geq 90\%$, Sigma) was used in the study of adsorption. The protein was dissolved in a high purity NaCl solution with a controlled ionic strength ($I = 0.001, 0.01, 0.15$ M). The protein solutions were used without additional purification.

2.2. Chromatography of LGB

Fast Protein Liquid Chromatography (FPLC) was used to analyze a mixture of A and B isoforms of bovine LGB. Separation of the isoform mixture was carried out using the ion-exchange chromatography method with the FPLC ÄKTA purifier system (GE Healthcare).

Separation was performed on a MonoQ GL 5/50 anion exchange column (GE Healthcare) at a flow rate of 2 ml/min at room temperature. For the separation process, high purity deionized water and 0.7 M sodium acetate with pH 6.3 were used [25].

2.3. UV-vis measurements

The LGB adsorption spectrum was measured for protein solutions at concentrations of 1–1000 ppm at an ionic strength of $I = 0.001$ M NaCl, using a UV-vis Evolution 300 spectrophotometer (Thermo Scientific) at wavelengths from 190 to 1100 nm.

2.4. Density measurements

The density of LGB solutions was measured using a DMA 5000 M density meter (Anton Paar), which is based on the oscillating U-tube method. The measurements were conducted for a concentration range from 100 to 7000 ppm at pH 6.5 and ionic strength of $I = 0.001$ M NaCl at 25 °C.

2.5. Viscosity measurements

Viscosity was measured using a Lovis 2000 M/ME rolling ball microviscometer (Anton Paar). The apparatus measured viscosity in the range from 0.3 to 10,000 mPa·s with an accuracy of 0.05%. Measurements on LGB solutions were conducted for a concentration range from 100 to 7000 ppm at an ionic strength of $I = 0.001$ M NaCl at 25 °C.

2.6. Dynamic light scattering and electrophoretic mobility measurements

The size of LGB molecule was measured with the dynamic light scattering (DLS) method using Zetasizer Nano ZS (Malvern). This technique measures the time-dependent fluctuations in the intensity of scattered light that occur because particles undergo Brownian motion. The analysis of these intensity fluctuations enables the determination of the diffusion coefficients of particles, which are converted into a size distribution.

The electrophoretic mobility of LGB solutions was measured using the Doppler effect (LDV – Laser Doppler Velocimetry). The results were used to determine zeta potential and isoelectric point (i.e.p.) of the studied protein.

The hydrodynamic diameter and electrophoretic mobility of LGB at a concentration of 1000 ppm in a NaCl electrolyte solution were measured for three ionic strengths ($I = 0.001$ M, $I = 0.01$ M, $I = 0.15$ M) at pH ranging from 2 to 10.

2.7. Quartz crystal microbalance with dissipation (QCM-D)

Adsorption of the protein on a gold surface was monitored using a quartz crystal microbalance with energy dissipation monitoring (Q-Sense E1, Biolin Scientific). The flow rate in the measurement system was controlled via a peristaltic pump. The baseline was determined by a 10 min flow of NaCl solution with an appropriate ionic strength. Adsorption of the protein at a concentration of 5 ppm was conducted for $t = 90$ min. After adsorption, the system was rinsed with a NaCl solution of specified ionic strength for $t = 90$ min. Adsorption was conducted at a pH ranging from 3.5 to 9, the pH was adjusted by the addition of high purity HCl or NaOH. The measurements were conducted at 25 °C.

2.8. Surface zeta potential of gold QCM-D sensor

The surface zeta potential of macroscopic solids such as the gold sensor used in the QCM-D experiments is commonly determined from the streaming potential measurements using the classical Helmholtz-Smoluchowski equation

$$\zeta = \frac{dU_{str}}{d\Delta p} \times \frac{\eta}{\varepsilon \times \varepsilon_0} \times \kappa_B \quad (1)$$

where $dU_{str}/d\Delta p$ is the streaming potential coefficient, η and ε are the viscosity and dielectric coefficient of water, ε_0 is the vacuum permittivity, and κ_B is the electric conductivity of the aqueous solution. According to Eq. (1) the streaming potential, which is a d.c. voltage generated by the flow of an aqueous solution through a capillary surrounded by the sample surface gets compensated by the bulk conductivity of the electrolyte solution. The approximation of the conductance of the flow channel by the bulk conductivity is valid for the zeta potential analysis of non-conductive material surfaces. However, in the case of the gold sensor, the QCM-D quartz disk is covered by a conductive gold layer, which serves as the adsorbent surface but also as the electrode for activating the sensor oscillation in the QCM-D experiment. The additional conductance introduced by the gold surface and its effect on the streaming potential coefficient are not considered by Eq. (1) and commonly lead to an *apparent* zeta potential only. Therefore the alternative approach for surface zeta potential analysis, i.e., the measurement of

streaming current, was used instead. The zeta potential is then calculated according to

$$\zeta = \frac{dl_{str}}{d\Delta p} \times \frac{\eta}{\varepsilon \times \varepsilon_0} \times \frac{L}{A} \quad (2)$$

where $dl_{str}/d\Delta p$ is the streaming current coefficient, and L and A are the lengths and the cross-section of the flow channel. The knowledge of the cell constant L/A of the flow channel restricts the application of Eq. (2) to the zeta potential analysis in single capillaries with a regular cross-section, e.g., circular, square, or rectangular. Two gold sensors (14 mm diameter, 300 μm thickness) are mounted opposite of each other inside the Adjustable Gap Cell for 14 mm Disks and separated by a distance of approx. 100 μm . This sample arrangement introduces a flow channel, whose shape may be approximated by a rectangular channel. Although the average length and width estimate a cell constant $L/A = 1$, calibration with a non-conductive polymer show $L/A = 1.5$. Such calibration is based on the fact that for a non-conductive material surface, the zeta potential results calculated from Eqs. (1) and (2) coincide (provided that the ionic strength is high enough to suppress any contribution of interfacial conductance).

The streaming current was sensed by highly reversible Ag/AgCl electrode. The zeta potential of gold sensors was determined in an aqueous solution of 0.01 M NaCl at different pH adjusted with 0.05 M HCl and 0.05 M NaOH, respectively. Throughout the series of surface zeta potential analyses, the electrolyte solution was continuously purged with nitrogen (N_2 5.0) to prevent dissolution of carbon dioxide (CO_2) from the ambient.

To evaluate the effect of frequent sensor cleaning after each QCM-D experiment and to confirm the absence of Na^+ and Cl^- ion adsorption, measurements were also performed in 0.001 M NaCl and for new and used gold sensors.

3. Results and discussion

3.1. Physicochemical properties of LGB

The crystal structure of LGB has been reported by several groups. Similar to other proteins of the lipocalin family, the core of the molecule

is an eight-stranded up-and-down beta-barrel comprising of beta-strands A to H (Fig. 1) [26].

The ninth beta-strand (I) is responsible for dimerization [1,27–29]. The long hydrophobic pocket located inside the beta-barrel is the primary ligand-binding site. The entrance to the binding pocket is surrounded by the flexible loops: AB, CD, EF and GH, whereas loops BC, DE and FG are located at the bottom of the beta-barrel [30]. Small fragments of the LGB chain consist of three alpha-helices [31]. Ligand binding in the beta-barrel has been confirmed by numerous crystal structures. However, the presence of alternative binding sites has already been postulated. Among them are the hydrophobic groove between alpha-helix and beta-barrel, a surface site near the entrance to the beta-barrel close to Trp19-Arg124, and the dimerization interface [1,28]. Only the first site has been confirmed by the crystal structure of LGB with vitamin D_3 [32].

LGB was the first protein in which polymorphism was found, and ten isoforms have been identified. The two prevalent isoforms of LGB in milk, isoforms A and B, differ by two amino acid substitutions: Asp64 and Val118 in isoform A are replaced in isoform B with glycine and alanine, respectively [33,34]. Even though the primary structure is different for isoforms A and B, the studies performed by circular dichroism and X-ray diffraction proved that both variants have the same three-dimensional structure [35,36]. To determine the ratio between individual isoforms, present in the purchased preparation, the FPLC method was used (Fig. S1). Based on the surface area of the peak, the LGB-A to LGB-B ratio was found to be 2:1.

The UV-vis study showed that the LGB spectrum in the UV range has two maxima (Fig. S2). The maximum at a wavelength of 193 nm is assigned to the peptide bond, whereas the absorption in the 260–290 nm range with a maximum at 278 nm originates from aromatic residues of amino acids, mainly Trp and Tyr, in the polypeptide chain. An LGB molecule has Trp residues at positions 19 and 61, and Tyr residues at positions 20, 42, 99 and 102. The absorption value of the LGB solution in the studied concentration range (from 1 ppm to 100 ppm) increased from 0.01 to 0.12 in accordance with the Beer-Lambert law, with a maximum at 278 nm. At a wavelength of 193 nm, the absorbance ranges from 0.2 to 2.9.

The density of LGB solutions at concentrations from 100 to 7000 ppm was measured at an ionic strength of $I = 0.001$ M. The dependence of LGB solution density on LGB concentration is linear. The apparent

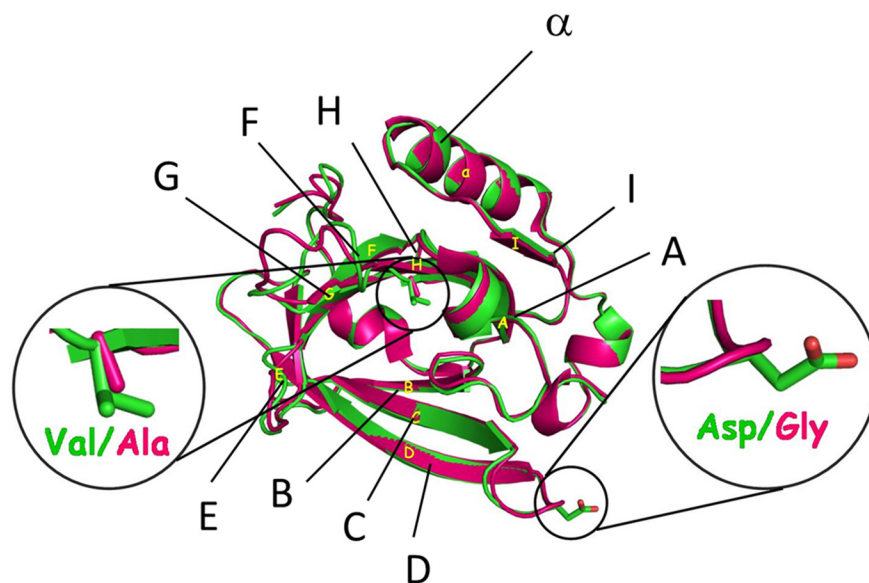


Fig. 1. Crystal structure of β -lactoglobulin with a cartoon representation of the secondary structure elements: beta-strands (letters A–I) and α -helix (α). The structure of isoform A (PDB ID: 4IB8) is shown in green, whereas pink color represents structure of isoform B (PDB ID: 4IBA).

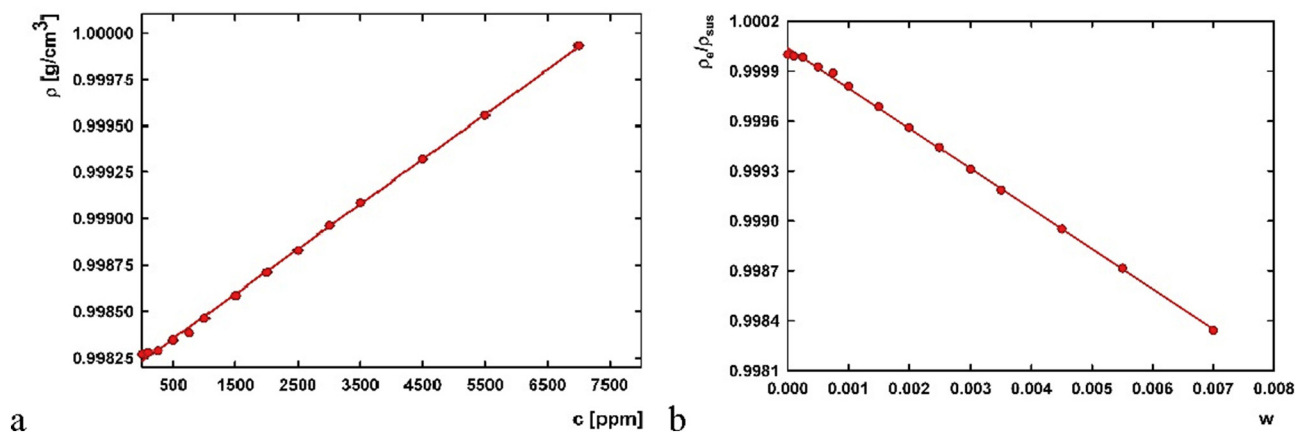


Fig. 2. a) LGB solution densities as a function of LGB concentration, b) LGB relative density (ρ_e/ρ_{sus}) as a function of weight fraction (w) for ionic strength $I = 0.001$ M NaCl at pH = 5.5.

protein density ρ_p was determined on the basis of the dependence of the relative density (ρ_e/ρ_{sus}) on the weight fraction (w) (Fig. 2) using the equation:

$$\rho_p = \frac{\rho_e}{1 + tg\alpha} \quad (3)$$

where ρ_e is the solvent density and $tg\alpha$ is the tangent of the relative density slope ρ_e/ρ_{sus} as a function of weight fraction.

The value of the LGB apparent density was found to be 1.32 g/cm^3 , which is close to 1.33 g/cm^3 , as reported by Renard [37].

The dynamic viscosity η and kinematic viscosity ν were measured at physiological pH in the concentration range of 100–7000 ppm at an ionic strength of 0.001 M. Both η and ν increase as protein concentration increases. The dynamic viscosity of LGB solutions at concentrations from 100 to 7000 ppm varied from 0.9913 to 1.0200 mPa·s, whereas the kinematic viscosity varied from 0.9927 to 1.0203 mm^2/s .

The diffusion coefficient of LGB was determined using the DLS method. From this value the hydrodynamic diameter (D_H) of LGB molecules was calculated from the Stokes equation:

$$D_H = \frac{kT}{3\pi\eta D} \quad (4)$$

where D is the diffusion coefficient, and η is the dynamic viscosity of water, k the Boltzmann constant, T the absolute temperature.

The hydrodynamic diameter of LGB molecules ranges from 4 nm to 7 nm for pH 2–10 and $I = 0.001$ –0.15 M. At a low ionic strength ($I = 0.001$ M), LGB monomers are present, whereas an increase in the solution ionic strength results in the formation of dimers. At

extreme pH values, aggregates with a radius of 700 nm and 1200 nm are present (Fig. 3). The size of aggregates increases with the solution's ionic strength. This is consistent with data reported in the literature, which shows that at pH 3.7–5.2, LGB irreversibly forms oligomers: this effect is greatest at pH 4.6 [3]. The tendency for aggregation is the consequence of the low charge of protein around the isoelectric point. At high pH >9.5 , protein lost natural structure and occurs in oligomeric denatured form.

It is advantageous to approximate the true protein shape by a prolate spheroid shape because its hydrodynamic radius can be calculated analytically using the expression [38]

$$R_H = \frac{a(\lambda^2 - 1)^{1/2}}{\cosh^{-1}\lambda} \quad (5)$$

where $\lambda = a/b$ is the aspect ratio parameter having major significance for predicting the hydrodynamic behavior of spheroidal particles, and b and a are the shorter and the longer semiaxes of the spheroid, respectively.

With the assumption of a prolate spheroid shape and Eq. (5), the LGB monomer ($4.0 \times 4.4 \times 3.7$ nm, $\lambda = 1.18$, $R_H = 2.56$ nm) and dimer ($7.7 \times 4.4 \times 4.2$ nm, $\lambda = 1.83$, $R_H = 3.23$ nm) have a hydrodynamic diameter of $D_H = 5.12$ nm and $D_H = 6.46$ nm, respectively. These calculated diameters are indicated as dashed horizontal lines in Fig. 3b.

Using laser Doppler velocimetry (LDV), electrophoretic mobility of protein solutions was measured in the pH range 2.5–10.5. Changes in the electrophoretic mobility of an LGB solution as a function of pH is shown in Fig. 4a for three ionic strengths. Thus determined electrophoretic mobility varies from -3.9 to $3.3 \times 10^{-8} \text{ m}^2(\text{V}\cdot\text{s})^{-1}$ and from -1.9

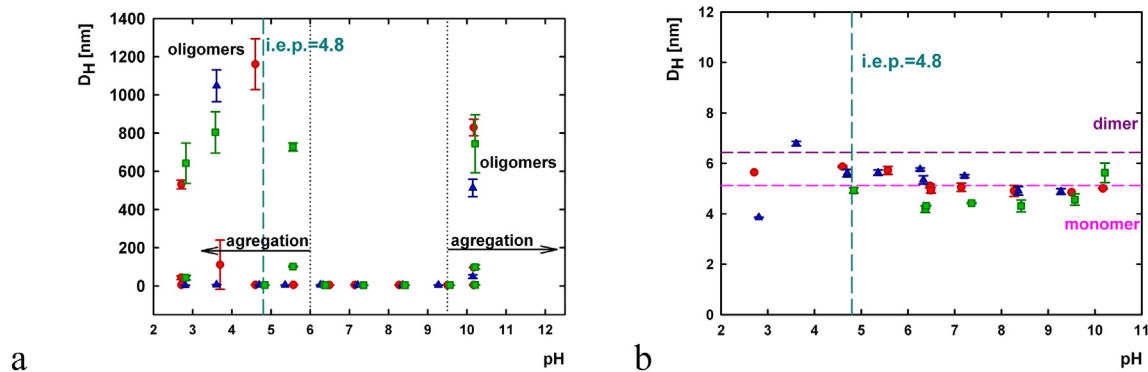


Fig. 3. Hydrodynamic diameter (D_H) of LGB molecules as a function of pH in the range 2–10 for $I = 0.001$ M (■ green), $I = 0.01$ M (● red) and 0.15 M (▲ blue). The dashed vertical line represents i.e.p., dotted lines in panel a shows the range below and above which LGB aggregates, dashed horizontal lines in panel b shows the D_H limits where LGB transfers from monomer to dimer according to Eq. (5).

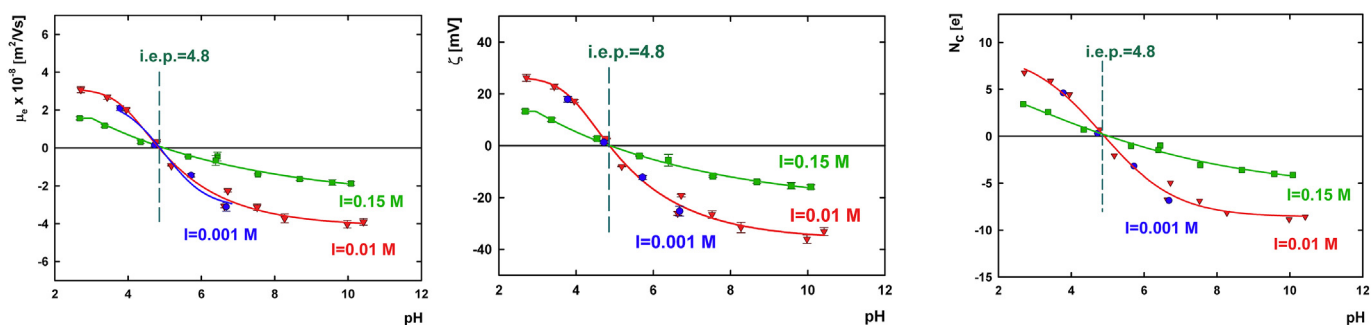


Fig. 4. Changes in a) electrophoretic mobility μ_e , b) zeta potential ζ of LGB and c) effective charge N_c of LGB as a function of pH for ionic strengths $I = 0.001$ M (● blue) $I = 0.01$ M (▼ red) and $I = 0.15$ M (■ green). The dashed line shows i.e.p. for LGB.

to $1.6 \times 10^{-8} \text{ m}^2(\text{V}\cdot\text{s})^{-1}$ for solutions with ionic strengths $I = 0.01$ M and $I = 0.15$ M, respectively. For ionic strength $I = 0.001$ M measurements were performed only in pH range from 3.5 to 6.5, and electrophoretic mobility varies from -3.0 to $2.0 \times 10^{-8} \text{ m}^2(\text{V}\cdot\text{s})^{-1}$.

The measured dependence of electrophoretic mobility on the solution pH and the hydrodynamic diameter made it possible to estimate the zeta potential of LGB molecules (Fig. 4b) from Henry's formula:

$$\zeta = \frac{3\eta\mu_e}{2\epsilon f(\kappa a)} \quad (6)$$

where ζ is the zeta potential, μ_e is the electrophoretic mobility, ϵ is the dielectric constant, η is the viscosity and $f(\kappa a)$ is Henry's function ($f(\kappa a) = 1.0$ for $I = 1 \times 10^{-3}$ M, 1.03 for $I = 1 \times 10^{-2}$ M, 1.1 for $I = 0.15$ M). The isoelectric point (i.e.p.) of LGB was also determined: it has the same value (pH 4.8) within the range of ionic strength studied. This value lies in the range of 4.7–5.2 reported in the literature [39–42]. As isoform A has i.e.p. located at higher pH than isoform B (the presence of an Asp residue at position 64 makes it slightly more negatively charged as compared to isoform B) [8], and taking into consideration that the studied preparation contained isoforms A and B in the ratio 2:1, the i.e.p. 4.8 is near the lower end of the range of values reported in the literature.

In solutions with an ionic strength of $I = 0.01$ M, zeta potential, ζ ranged from -33.3 to 26.5 mV, whereas in solutions with a higher ionic strength of $I = 0.15$ M, values of zeta potential ζ ranged from

-16.0 to 13.3 mV. The obtained zeta potential values show that the net charge of LGB molecules at $\text{pH} < 4.8$ is positive, whereas at $\text{pH} > 4.8$, the protein molecules are negatively charged.

The effective charge (q) of LGB was calculated from the electrophoretic mobility and the hydrodynamic radius using the Lorentz-Stoke equation:

$$q = \frac{kT}{D} \mu_e = 6\pi\eta R_H \mu_e \quad (7)$$

Taking into account the value of the elementary electric charge, $e = 1.602 \cdot 10^{-19}$ C, the average number of elementary charges per molecule, N_c , was calculated by:

$$N_c = \frac{6\pi\eta R_H}{e} \mu_e \quad (8)$$

In the range of pH 2.5–10.5, the value of N_c varied from -8.5 to 6.7 and from -4.2 to 3.4 in solutions with ionic strengths of $I = 0.01$ M and $I = 0.15$ M, respectively (Fig. 4c).

Isoform A (LGB-A) contains 47 charged amino acid residues (15 lysine residues, 3 arginine residues, 11 asparagine acids, 16 glutamic acids, 2 histidines), which can be protonated or deprotonated. In the molecule of isoform LGB-B, there are 46 charged amino acid residues, because the asparagine acid residue at position 64 is replaced by glycine. The positions of polar amino acid residues are shown in Fig. 5.

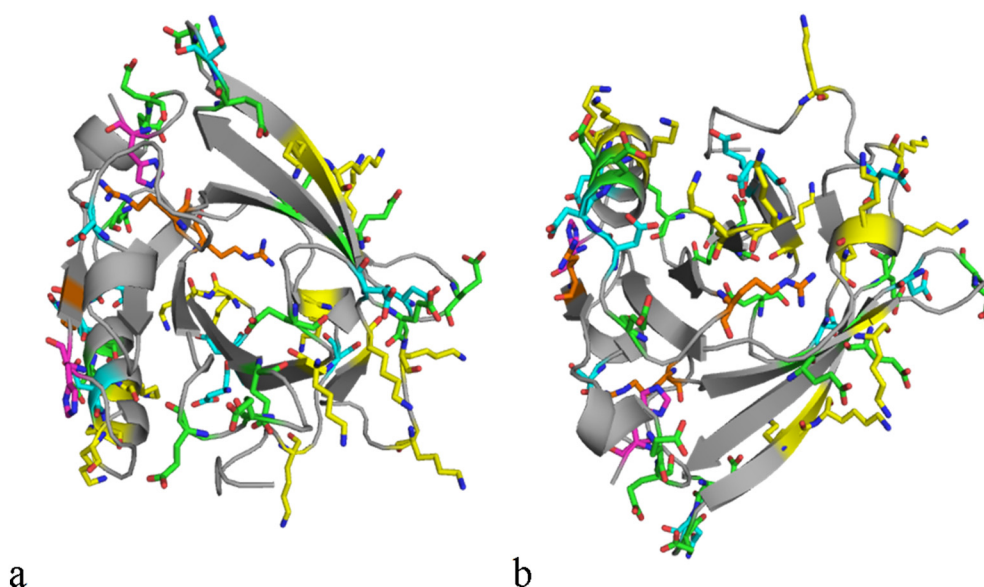


Fig. 5. Location of polar amino acid residues on LGB surface: glutamic acid (green), asparagine acid (blue), lysine (yellow), arginine (orange), histidine (pink) [PDB ID: 1BSQ].

The net charge of the LGB A molecule is $-8.7e$, whereas that of the LGB-B molecule is -7.7 (at pH 7.0). At pH values below the i.e.p., LGB molecules are protonated and the theoretical average charge in acidic solutions at pH = 3.5 is 17.3 (17.4 for LGB-B); in solutions with pH above i.e.p., LGB molecules donate protons and acquire a negative charge of -7.5 (-6.5 for LGB-B) at a native value of pH = 6.3, whereas in alkaline medium of pH = 9.5 the protein molecule has a charge of -19.3 (-18.1 for LGB-B) [43].

In analyzing the 3D structure of the studied protein and taking into consideration the modified number of charged amino acid residues, the nominal number of charges N_m was determined [44]. The effective ionization level α of the LGB molecule is equal to the ratio of the average number of elementary charges N_c to the nominal number of charges N_m in the molecule at a given pH, $\alpha = (N_c / N_m) \cdot 100\%$. At $\mu_e = -2.1 \times 10^{-8} \text{ m}^2(\text{V}\cdot\text{s})^{-1}$ ($I = 0.01 \text{ M}$, pH 6.3) and $R_H = 2.35 \text{ nm}$, N_c is equal to 5.2. As the nominal number of charges in an LGB molecule is 26 and 25 for LGB-A and LGB-B, respectively, the effective ionization level α is 20.0% for isoform A and 20.8% for isoform B. In a solution with ionic strength $I = 0.15 \text{ M}$, $\mu_e = 0.9 \times 10^{-8} \text{ m}^2(\text{V}\cdot\text{s})^{-1}$ (pH 6.3, $R_H = 2.4 \text{ nm}$, $N_c = 1.0$) the effective ionization level $\alpha = 4.0\%$ for isoform A and 3.8% for isoform B.

Both the nominal number of charges N_c and the effective ionization level strongly depend on the solution's ionic strength and pH. The value of the effective ionization level for a solution with an ionic strength of $I = 0.01 \text{ M}$ is five times higher than that for a solution with an ionic strength of $I = 0.15 \text{ M}$ at the same pH. The obtained value of the effective ionization level shows that the phenomenon of compensation of a nominal number of charges N_m occurs. In analyzing the protonation of a protein molecule, it is extremely important to know how charged amino acid residues are spatially arranged. The amino acid residues that affect the net charge can be located on the surface of the molecule or inside the molecule, which is of key importance for the exchange of protons and adsorption on the surface of protein molecule [24].

3.2. Zeta potential of gold surface

Fig. 6 shows the pH dependence of the surface zeta potential for the gold sensors used in the QCM-D adsorption experiments. The zeta potential was first determined at the native pH of the aqueous 0.01 M NaCl solution, i.e., at pH 5.5–6, followed by a titration with acid to obtain the i.e.p. The gold sensors were then maintained in the measuring cell,

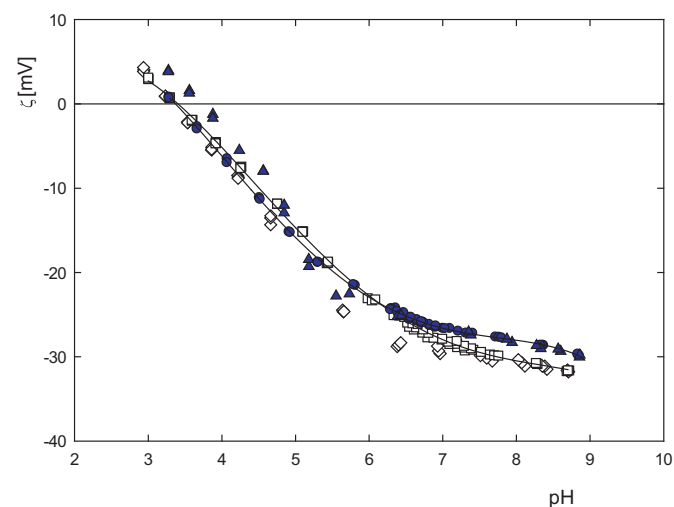


Fig. 6. pH dependence of zeta potential for pristine (\diamond , \square) and used-and-cleaned (Δ , \circ) gold sensor disks for QCM-D adsorption experiments determined in 0.01 M NaCl. Open squares (pristine sensor) and open circles (used sensor) represent the repeated titration from high to low pH.

rinsed with deionized water and the streaming current was repeatedly measured in fresh 0.01 M NaCl before titration to high pH. Subsequently, the titration was reversed again now starting at high pH and proceeding towards the i.e.p. again.

The change of the electrolyte solution and the exposure of the gold surface to water and acidic conditions do not affect the zeta potential, which confirms the high stability and chemically inert behavior of gold in aqueous surroundings. The titration from high to low pH, however, shifts the i.e.p. from pH 3.7 to slightly lower pH 3.4. We assume that carbonate ions dissolved in the NaOH stock solution accumulate at the gold surface and drive the gold-water interface more acidic. The nitrogen purge of the electrolyte solution, which is continuously applied throughout the measurement, is little effective to remove CO_3^{2-} ions. On the other hand, we observe a reproducible i.e.p. at pH 3.3 for pristine gold sensors but again a shift in the i.e.p. similar to the used sensors for a measurement in 0.001 M KCl (Fig. S4). Schrems et al. [45] reported an i.e.p. 2.9 for gold sensors measured in an aqueous 0.001 M KCl solution and a zeta potential of $\zeta = -33 \text{ mV}$ at pH 5.6. The zeta potential at pH 5.6 matches the result obtained for pristine gold sensors in 0.001 M KCl (Fig. S3) but the i.e.p. reported by Schrems et al. is further shifted to lower pH due to the missing nitrogen purge of the electrolyte solution. At the higher ionic strength of 0.01 M, the double layer at the gold-water interface gets further compressed and the decline of the double layer potential is steeper. The effect of ionic strength in the range of 0.001–0.01 M on the zeta potential of gold is more pronounced than the corresponding effect on LGB. The contribution of interfacial charge introduced by the adsorption of water ions (hydroxide, OH^- , and hydronium, H_3O^+) on the gold surface adds to the explanation of this difference [46].

Besides the interfacial charge by adsorbed water ions, the quartz surface, which remains uncovered by the gold electrode surface of the QCM-D sensor and thus gets exposed to the aqueous solution, is expected to contribute to the surface zeta potential of gold sensors. The outer quartz ring of the sensors has a width of 1 mm, which makes their total surface composed of 73.5% gold and 26.5% quartz. The i.e.p. for fused silica is reported at pH 2.9 [47]. Assuming the same surface roughness for the quartz substrate and the thin-film gold coating, the specific surface areas for SiO_2 and Au are equal to the corresponding geometric areas, and the assumption of area-weighted contributions of quartz and gold to the as determined zeta potential ζ_{measured} applies. The correct zeta potential of gold may then be calculated according to [48].

$$\zeta_{\text{measured}} = x \zeta_{\text{gold}} + (1-x) \zeta_{\text{quartz}} \quad (9)$$

with $x = 0.735$.

The i.e.p. for solely the gold surface of the QCM-D sensor, which is experienced by LGB during the adsorption experiment, is then estimated at pH 4 and thus matching the i.e.p. of material surfaces that lack functional groups [46].

In summary the gold surface and gold-water interface, respectively, is positively charged below the experimentally determined i.e.p. 3.5 and negatively charged above the calculated i.e.p. 4. Below pH 3.5 and above pH 4.8 (i.e., the i.e.p. of LGB), LGB and gold are equally charged whereas in the range of pH 3.5–4.8, protein and adsorbant surface assume an opposite charge. The relative charging behavior is reflected by the kinetics and efficiency of LGB adsorption on gold discussed in the next section.

3.3. LGB adsorption on gold surface

Adsorption of LGB onto a gold surface was studied by QCM-D. The measurements were conducted in NaCl electrolyte solutions with ionic strengths of 0.001, 0.01 and 0.15 M (Fig. S4). The solution concentration of LGB used during adsorption was 5 ppm. To characterize the effect of pH on the LGB adsorption on the gold surface, measurements were conducted at pH ranging from 3.5 to 9.5.

Adsorption of LGB onto the QCM-D sensor surface results in a considerable decrease in Δf and a slight increase in ΔD over time, where Δf and ΔD are the changes in the frequency and dissipation of the oscillating QCM-D sensor, respectively. The registered curves of the dependence of Δf and ΔD on time of protein adsorption in 0.001 M NaCl at different pH are shown in Fig. 7. The curves have a similar shape: the greatest changes in Δf take place in the initial phase of the experiment, the maximum occurs for moderately acidic medium, whereas when the pH of the LGB solution exceeds the i.e.p., the value of Δf gradually, but significantly decreases. In a solution with an ionic strength of $I = 0.001$ M at pH ranging from 3.5 to 4.5, the resonance frequency reaches the lowest value; whereas with increasing pH in a range from 5.5 to 9.5, a strong decrease in Δf takes place. The values of Δf in solutions with ionic strengths of 0.01 and 0.15 M (Fig. S4) also decrease with an increase in pH in the range of 5.5–9.5, but this decrease is not as distinct as in the experiment conducted at an ionic strength of 0.001 M. An increase in the ionic strength causes screening of the protein charge, which consequently leads to a decrease in repulsive electrostatic forces between protein molecules, thus facilitating the formation of a packed adsorption layer on the sensor surface.

When the system is rinsed after adsorption with NaCl solution, it does not cause significant changes in Δf or ΔD ; this shows that irreversible adsorption of LGB occurs. At an ionic strength of $I = 0.15$ M, only 2–5% of the proteins desorb, whereas at smaller ionic strengths ($I = 0.01$ M, $I = 0.001$ M) desorption ranges from 15 to 25% of the protein, depending on pH.

In all experiments conducted at different values of pH and ionic strength, the LGB layers are characterized by a small dissipation ($\Delta D < 1 \times 10^{-6}$) which shows that the layers of adsorbed protein are rigid. From the resonance frequency values, using the Sauerbrey model, the mass of adsorbed LGB layer was found. The Sauerbrey model describes the linear dependence between the resonance frequency and the mass adsorbed onto the sensor surface, as described by:

$$\Gamma = -C \frac{\Delta f}{n} \quad (10)$$

where Γ is the adsorbed mass (ng/cm^2), C is the sensor constant ($17.7 \text{ ng}/\text{cm}^2$), Δf is the change in the resonance frequency, and n is the overtone mode.

The decrease in the resonance frequency corresponds to the increase in the adsorbed mass. The Sauerbrey model is in good agreement with the measurements when used to describe “rigid layers” which are characterized by low dissipation. In all our experiments (at ionic strengths from 0.001 to 0.15 M), the greatest values of adsorbed protein mass were observed at acidic pH values about 3.5–4.5, whereas at pH 5.5–9.5, a distinct decrease in the mass of adsorbed LGB can be observed. The maximum value of Γ_{LGB} at individual ionic strengths is

$232.6 \pm 1.1 \text{ ng}/\text{cm}^2$ for $I = 0.001$ M, $264.7 \pm 1.3 \text{ ng}/\text{cm}^2$ for $I = 0.01$ M and $307.8 \pm 1.4 \text{ ng}/\text{cm}^2$ for $I = 0.15$ M, which shows that the mass of adsorbed protein increases with an increase in the solution ionic strength. The maximum of the adsorbed protein mass is often observed for solutions with pH close to the protein's isoelectric point [49,50].

From the QCM-D results, it can be inferred that β -lactoglobulin is more strongly adsorbed at pH values below its i.e.p., which is associated with the dominant role of electrostatic interactions [10,14]. Positively charged LGB molecules interact with the negatively charged sensor surface. This demonstrates the generally observed fact that adsorption is favored when the protein and the surface have opposite charges because electrostatic attraction facilitates migration of protein molecules towards the surface [14,51]. At pH values above the i.e.p. of LGB, both the protein molecule and the gold surface are negatively charged: in spite of this, LGB is adsorbed on the surface of gold by means of interactions with positive domains on the protein surface. In this case, however, the intensity of adsorption is much smaller. This shows that in LGB adsorption, hydrophobic forces have a smaller effect than electrostatic forces.

It is known from the literature that LGB occurs in the form of monomers or dimers – depending on the environmental conditions. The dimensions of monomer and dimer molecules are: $4.0 \text{ nm} \times 4.4 \text{ nm} \times 3.7 \text{ nm}$ and $7.7 \text{ nm} \times 4.4 \text{ nm} \times 4.2 \text{ nm}$ [34,52,53], and their molecular weights are 18.3 kDa and 36.6 kDa, respectively. Using the Random Sequential Adsorption (RSA) model for an ellipsoid [54], the surface excess Γ_{LGB}^{RSA} was determined for an LGB monolayer by:

$$\Gamma_{LGB}^{RSA} = \frac{M_{LGB}}{n_a \cdot A_{LGB}} \cdot \Theta^{RSA} \quad (11)$$

with

$$A_{LGB}^{sideonab} = \pi \cdot a \cdot b \quad (12)$$

where a , b and c are the ellipsoid semi-axes, Γ_{LGB}^{RSA} is the theoretical surface excess [ng/cm^2], n_a is the Avogadro number, M_{LGB} is the molecular weight of LGB, A_{LGB} is a parallel projection of the ellipsoid and Θ^{RSA} is the maximum surface coverage. The values of Θ^{RSA} were determined using the RSA model for an ellipsoid [54]. The calculated values of the surface excess for various orientations of LGB molecules in a monolayer are given in Table 1.

The calculated values of Γ_{LGB}^{RSA} for all orientations of the monomer and for the dimer in the side-on orientation are similar, and their average values ($\Gamma_{LGB_{av}}^{RSA}$) are $135.0 \text{ ng}/\text{cm}^2$ and $136.8 \text{ ng}/\text{cm}^2$, respectively; the value for the dimer in the end-on orientation is almost twice that high and is equal to $269.5 \text{ ng}/\text{cm}^2$.

Peraz-Fuentez [14] based on MD simulation, QCM-D and AFM measurements determined that LGB creates rigid layers on the surface with

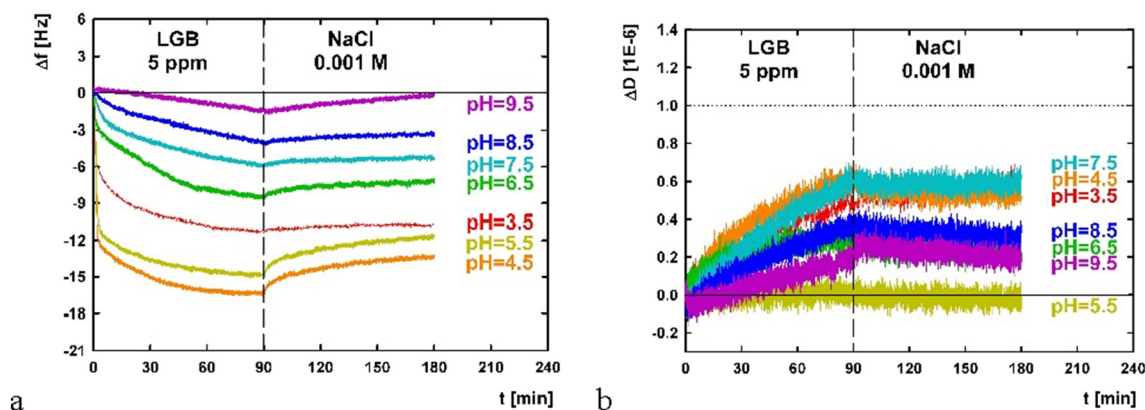

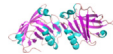



Fig. 7. Resonance frequency (Δf) and dissipation (ΔD) as a function of time (t) for ionic strength $I = 0.001$ M. The dashed line shows the end of LGB adsorption after $t = 90$ min and rinsing the sensor with an electrolyte solution.

Table 1
Surface excess Γ_{LGB}^{RSA} for an LGB monomer and dimer.

	Monomer	Dimer	End on
Dimension [nm]	$4.0 \times 4.4 \times 3.7$	$7.7 \times 4.4 \times 4.2$	
M_{LGB} [kDa]	18.3	36.6	
Orientation	Side on/end on	Side on	End on
Structure			
b/a	0.84–0.93	0.54–0.57	0.54
A_{LGB} [nm ²]	11.6–13.8	25.4–26.6	14.5
Θ^{RSA}	0.560–0.570	0.585	0.565
Γ_{LGB}^{RSA} [ng/cm ²]	123.1–146.4	133.6–140.0	269.5
$\Gamma_{LGB_{av}}^{RSA}$ [ng/cm ²]	135.0 ± 11.7	136.8 ± 4.5	269.5
$\Gamma_{LGB_{av}}^{RSA} + 50\% \text{ H}_2\text{O}$ [ng/cm ²]	270.0 ± 23.0	273.6 ± 9.0	539.0

M_{LGB} – molecular weight, b/a – ellipsoid elongation (b and a are the shorter and the longer semiaxes of the spheroid), A_{LGB} – parallel projection of the ellipsoid, Θ^{RSA} – maximum surface coverage [55], Γ_{LGB}^{RSA} – surface excess, $\Gamma_{LGB_{av}}^{RSA}$ – average surface excess, $\Gamma_{LGB_{av}}^{RSA} + 50\% \text{ H}_2\text{O}$ average surface excess taking into account H₂O.

a thickness of 3 nm, and the surface area occupied by the protein molecule is equal to 14.4 nm².

Using the VMD software and the structural data (PDB ID: 1BEB), a graphical representation of the LGB molecule dipole moment was generated (Fig. S5). The distribution of charges shows that the LGB molecule is characterized by a heterogeneous distribution of charges on the surface [55–58]. In the modelled structures, the vector of the LGB dipole moment runs along β -sheets of B, C, D, and the direction from the negatively charged area to the positively charged area coincides with the direction of sheets B, D. In the case of a dimer molecule, the dipole moment is oriented perpendicular to sheet I which is the place where the monomers contact each other, and then runs towards the alpha helix. The dipole moments of the monomer and dimer have different directions, which show that other amino acid residues are responsible for the adsorption of monomers and dimers. The value of the dipole moment in the model structures calculated using the VMD software is 665 D for the monomer and 997 D for the dimer at pH 7.4.

The dependence of the adsorbed mass of LGB on pH for the studied ionic strengths is shown in Fig. 8. The values of $\Gamma_{LGB_{av}}^{RSA}$ for individual orientations of the LGB molecules in the adsorbed layers are also indicated. The dashed line represents the mass of an LGB monolayer (Γ_{LGB}), whereas the green dashed line represents the adsorbed mass taking into account water molecules present in the adsorbed layer $\Gamma_{LGB_{av}}^{RSA} + 50\% \text{ H}_2\text{O}$ for individual orientations. Based on the paper by Pessen

et al., it can be concluded that the hydration level of the LGB layer is about 50% [59].

Taking into consideration that the adsorbed mass also includes water molecules, the value of the adsorbed mass at a level of 232–307 ng/cm² shows that the molecules have a side-on orientation on the surface of gold. The existence of the side-on orientation is not only inferred from the QCM-D data but is also confirmed by MD simulations, which show the preferential orientation of molecules.

As shown by the QCM-D results, the process of LGB adsorption on the surface of gold is mainly affected by electrostatic interactions. The dependence of the adsorbed LGB mass on the zeta potential of protein is shown in Fig. S6. The graph shows a strong correlation between the charge and the effectiveness of protein adsorption. The values of LGB mass adsorbed at the same zeta potential but at different ionic strengths are similar. Also, the LGB mass adsorbed at positive zeta potential values is >200 ng/cm², whereas that of negatively charged LGB molecules is smaller than 200 ng/cm². For the sake of comparison, it is worthwhile tracing changes in the zeta potential of the gold surface. The gold sensor is highly negatively charged at a high pH and weakly negatively charged at low pH. The i.e.p. for the gold surface is near pH 3.5. In the pH range 7.0–9.0 the zeta potential of gold is about –30 mV (see Fig. 6). Complex asymmetric structure of the protein molecule affects its adsorption process. Positively charged fragments of the molecule are oriented towards the negatively charged gold surface. Under these conditions, electrostatic attraction effectively immobilizes the protein molecule. In the case of pH >4.8, both the LGB and the gold surface are negatively charged, which is reflected in the decrease in protein adsorption to the gold surface. The most effective protein immobilization occurs in the range between pH 3.5–4.8 when the protein is positively charged, and the surface simultaneously has a negative charge, which is confirmed by QCM-D results (Figs. 8 and S6).

Also, based on the QCM-D results, the thickness of the adsorbed layer can be assessed using formula $d_{eff} = \Gamma_{LGB} / \rho_{eff}$. Assuming that water accounts for 50% of protein weight and knowing the LGB apparent density $\rho_{LGB} = 1.32 \text{ g/cm}^3$ the effective density was calculated as $\rho_{eff} = 1.16 \text{ g/cm}^3$. The maximum effective thickness of the layer adsorbed on gold surface was calculated for the ionic strength in the range 0.001–0.15 M at pH = 4.5, which is equal to 2.0 nm for $I = 0.001 \text{ M}$, 2.3 nm for $I = 0.01 \text{ M}$ and 2.7 nm for $I = 0.15 \text{ M}$. These values show that the thickness of the layer clearly increases with the ionic strength of the solutions. The calculated values of the effective thickness of LGB layers adsorbed on the sensor are smaller than the thickness of a monomeric molecule (3.7 nm). These values are very close to the values 3 nm obtained using AFM for LGB film on polystyrene surface [14]. During adsorption, protein molecules are flattened as a result of interaction with the gold surface.

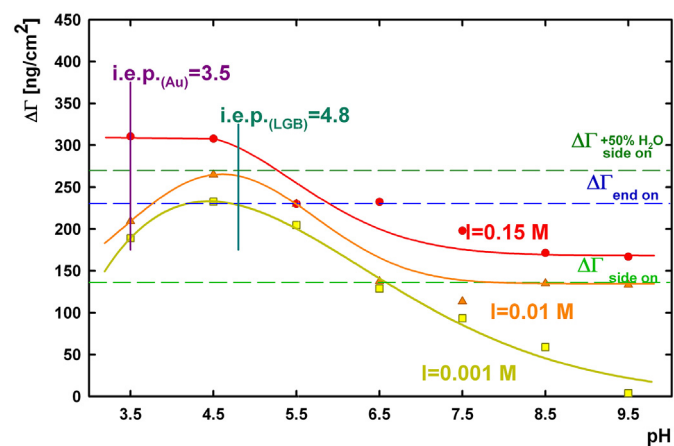


Fig. 8. Adsorbed mass Γ_{LGB} [ng/cm²] determined from QCM-D as a function of pH for three ionic strengths: $I = 0.001 \text{ M}$ (■ yellow), $I = 0.01 \text{ M}$ (▲ orange) and $I = 0.15 \text{ M}$ (● red) - The horizontal dashed lines represent the adsorbed mass Γ_{LGB} calculated by Eq. (10) for the monomer and dimer in the side-on orientation (green) and for the dimer in the end-on orientation (blue). The vertical line represents i.e.p. for LGB and gold surface.

4. Conclusions

Studies using dynamic light scattering have confirmed the tendency of LGB to create oligomeric forms. The hydrodynamic radius of LGB molecules varies from 4 nm to 7 nm for pH ranging from 2 to 10 and an ionic strength of 0.001–0.15 M. The obtained values demonstrate that monomeric and dimeric LGB forms are present in the solution. Also, at pH values below 6 and above 10, the presence of oligomeric forms with a radius of 700 nm and 1200 nm is observed.

The zeta potential of LGB varies from -33.3 mV to 26.6 mV for $I = 0.01$ M and from -16.5 mV to 13.4 mV for $I = 0.15$ M at the pH ranging from 2 to 10. The isoelectric point occurs at pH 4.8. The maximum effective ionization level of the LGB molecule is about 20% for ionic strength $I = 0.01$ M and 4% for $I = 0.15$ M, which shows that surface charge gets more compensated by the accumulation of oppositely charged ions in the Stern layer at higher ionic strength.

LGB adsorption on the surface of gold was monitored using the QCM-D method. LGB layers on the surface of gold are characterized by low dissipation of energy ($\Delta D < 1 \times 10^{-6}$). This shows that rigid layers are formed. Regardless of the ionic strength, the maximum values of the adsorbed mass Γ_{LGB} were obtained at pH 3.5–4.5. With an increase in pH, Γ_{LGB} decreases, and this effect is the greatest at an ionic strength of $I = 0.001$ M. The greatest effectiveness of adsorption occurs at an ionic strength of $I = 0.15$ M: only 2–5% of the protein undergoes desorption, whereas at lower ionic strength as much as 15–25% LGB undergo desorption.

In general, it can be concluded that electrostatic interactions play the dominant role in LGB adsorption on the surface of gold. The mass adsorbed on the QCM-D sensor for positive values of the LGB zeta potential is >200 ng/cm², whereas for negatively charged LGB molecules the adsorbed mass is smaller than 200 ng/cm². Electric charge has a very non-homogeneous distribution on the LGB surface, which is proved by its high dipole moment $\mu_D = 665$ D for pH = 7.0. Based on the QCM-D results and the MD charge distribution, one can conclude that LGB molecules form a monolayer on the sensor surface; this monolayer consists of monomers or dimers in the preferred side-on orientation. The mechanism of LGB adsorption is of significant importance for determining the optimum conditions for immobilizing this protein on the gold surface. The binding properties of immobilized β -lactoglobulin can be used to design controlled protein structures for biomedical applications.

Acknowledgements

The research was performed in the framework of the Marian Smoluchowski Krakow Research Consortium - Leading National Research Centre (KNOW), which is supported by the Ministry of Science and Higher Education.

This work was supported by Grant NCN OPUS 2016/23/B/ST5/02788.

Appendix A. Supplementary data

Supplementary data to this article can be found online at <https://doi.org/10.1016/j.bioelechem.2018.01.010>.

References

- [1] S. Brownlow, J.H. Morais Cabral, R. Cooper, D.R. Flower, S.J. Yewdall, I. Polikarpov, A.C. North, L. Sawyer, Bovine β -lactoglobulin at 1.8 Å resolution—still an enigmatic lipocalin, *Structure* 5 (1997) 481–495.
- [2] K. Sakai, K. Sakurai, M. Sakai, M. Hoshino, Y. Goto, Conformation, and stability of thiol-modified bovine β -lactoglobulin, *Protein Sci.* 9 (2000) 1719–1729.
- [3] M. Gottschalk, H. Nilsson, H. Roos, B. Halle, Protein self-association in solution: the bovine β -lactoglobulin dimer and octamer, *Protein Sci.* 12 (2003) 2404–2411.
- [4] J. Loch, A. Polit, A. Gorecki, P. Bonarek, K. Kurpiewska, M. Dziedzicka-Wasylewska, K. Lewinski, Two modes of fatty acid binding to bovine β -lactoglobulin—crystallographic and spectroscopic studies, *J. Mol. Recognit.* 24 (2011) 341–349.
- [5] J.I. Loch, P. Bonarek, A. Polit, S. Świątek, M. Dziedzicka-Wasylewska, K. Lewiński, The differences in binding 12-carbon aliphatic ligands by bovine β -lactoglobulin isoform A and B studied by isothermal titration calorimetry and X-ray crystallography, *J. Mol. Recognit.* 26 (2013) 357–367.
- [6] L. Sawyer, *Advanced dairy chemistry, Volume 1A: Proteins: Basic Aspects*, 4th edition 2013, pp. 211–259.
- [7] J.I. Loch, P. Bonarek, A. Polit, M. Jabłoński, M. Czub, X. Ye, K. Lewiński, β -Lactoglobulin interactions with local anesthetic drugs – crystallographic and calorimetric studies, *Int. J. Biol. Macromol.* 80 (2015) 87–94.
- [8] U.M. Elofsson, M.A. Paulsson, T. Arnebrant, Adsorption of β -lactoglobulin A and B: effects of ionic strength and phosphate ions, *Colloids Surf. B: Biointerfaces* 8 (1997) 163–169.
- [9] H. Itoh, A. Nagata, T. Toyomasu, T. Sakiyama, T. Nagai, T. Saeki, K. Nakanishi, Adsorption of β -lactoglobulin onto the surface of stainless steel particles, *Biosci. Biotechnol. Biochem.* 59 (1995) 1648–1651.
- [10] S. Blake, S. Amin, W. Qi, M. Majumdar, E.N. Lewis, Colloidal stability & conformational changes in β -lactoglobulin: unfolding to self-assembly, *Int. J. Mol. Sci.* 16 (2015) 17719–17733.
- [11] C.A.-C. Karlsson, M.C. Wahlgren, A.C. Trägårdh, β -Lactoglobulin fouling and its removal upon rinsing and by SDS as influenced by surface characteristics, temperature and adsorption time, *J. Food Eng.* 30 (1996) 43–60.
- [12] M. Wahlgren, T. Arnebrant, Adsorption of β -lactoglobulin onto silica, methylated silica, and polysulfone, *J. Colloid Interface Sci.* 136 (1990) 259–265.
- [13] K.D. Caldwell, J. Li, J.-T. Li, D.G. Dalgleish, Adsorption behavior of milk proteins on polystyrene latex. A study based on sedimentation field-flow fractionation and dynamic light scattering, *J. Chromatogr. A* 604 (1992) 63–71.
- [14] L. Pérez-Fuentes, C. Drummond, J. Faraudo, D. Bastos-González, Adsorption of milk proteins (b-casein and β -lactoglobulin) and BSA onto hydrophobic surfaces, *Materials* 10 (2017) 893.
- [15] J.C. Kim, D.B. Lund, Kinetics of beta-lactoglobulin adsorption onto stainless steel surfaces, *Biotechnol. Prog.* 14 (1998) 951–958.
- [16] M. Rabe, D. Verdes, S. Seeger, Understanding protein adsorption phenomena at solid surfaces, *Adv. Colloid Interface Sci.* 162 (2011) 87–106.
- [17] B.S. Murray, C. Deshaies, Monitoring protein fouling of metal surfaces via a quartz crystal microbalance, *J. Colloid Interface Sci.* 227 (2000) 32–41.
- [18] X. Qiao, X. Zhang, Y. Tian, Y. Meng, Progresses on the theory and application of quartz crystal microbalance, *Appl. Phys. Rev.* 3 (2016), 031106.
- [19] B. Jachimska, K. Tokarczyk, Combining surface plasmon resonance and quartz crystal microbalance to determine hydration of dendrimer monolayers, *J. Phys. Chem. C* 120 (2016) 19678–19685.
- [20] J. Saikia, B. Saha, G. Das, Interpreting the adsorption of serum albumin and lactoglobulin onto ZnS nanoparticles: effect of the conformational rigidity of the proteins, *J. Colloid Interface Sci.* 416 (2014) 235–242.
- [21] V. Lebec, J. Landoulsi, S. Boujday, C. Poleunis, C.-M. Pradier, A. Delcorte, Probing the orientation of β -lactoglobulin on gold surfaces modified by alkyl thiol self-assembled monolayers, *J. Phys. Chem. C* 117 (2013) 11569–11577.
- [22] B. Jachimska, K. Tokarczyk, M. Łapczyńska, A. Puciul-Malinowska, S. Zapotoczny, The effect of solution pH on the structure of bovine serum albumin adsorbed on the silica surface investigated by quartz crystal microbalance (QCM), *Colloids Surf. A Physicochem. Eng. Asp.* 489 (2016) 163–172.
- [23] B. Jachimska, A. Pajor, Physico-chemical characterization of bovine serum albumin in solution and as deposited on surfaces, *Bioelectrochemistry* 87 (2012) 136–146.
- [24] B. Jachimska, A. Kozłowska, A. Pajor-Swierzy, Protonation of lysozymes and its consequences for the adsorption onto a mica surface, *Langmuir* 28 (2012) 11502–11510.
- [25] T.R. Neyestani, M. Djalali, M. Pezeshki, Isolation of α -lactalbumin, β -lactoglobulin, and bovine serum albumin from cow's milk using gel filtration and anion-exchange chromatography including evaluation of their antigenicity, *Protein Expr. Purif.* 29 (2003) 202–208.
- [26] D.R. Flower, A.C.T. North, C.E. Sansom, The lipocalin protein family: structural and sequence overview, *Biochim. Biophys. Acta Protein Struct. Mol. Enzymol.* 1482 (2000) 9–24.
- [27] S. Uhrinová, M.H. Smith, G.B. Jameson, D. Uhrin, L. Sawyer, P.N. Barlow, Structural changes accompanying pH-induced dissociation of the β -lactoglobulin dimer, *Biochemistry* 39 (2000) 3565–3574.
- [28] G. Kontopidis, C. Holt, L. Sawyer, The ligand-binding site of bovine β -lactoglobulin: evidence for a function? *J. Mol. Biol.* 318 (2002) 1043–1055.
- [29] K. Sakurai, Y. Goto, Manipulating monomer-dimer equilibrium of bovine β -lactoglobulin by amino acid substitution, *J. Biol. Chem.* 277 (2002) 25735–25740.
- [30] G. Kontopidis, C. Holt, L. Sawyer, Invited review: β -lactoglobulin: binding properties, structure and function, *J. Dairy Sci.* 87 (2004) 785–796.
- [31] B.Y. Qin, M.C. Bewley, L.K. Creamer, E.N. Baker, G.B. Jameson, Functional implications of structural differences between variants A and B of bovine β -lactoglobulin, *Protein Sci.* 8 (1999) 75–83.
- [32] M.C. Yang, H.H. Guan, M.Y. Liu, Y.H. Lin, J.M. Yang, W.L. Chen, C.J. Chen, S.J. Mao, Crystal structure of a secondary vitamin D3 binding site of milk beta-lactoglobulin, *Proteins* 71 (2008) 1197–1210.
- [33] L. Sawyer, G. Kontopidis, S.Y. Wu, β -Lactoglobulin – a three-dimensional perspective, *Int. J. Food Sci. Technol.* 34 (1999) 409–418.
- [34] J. Godovac-Zimmermann, I. Krause, M. Baranyi, S. Fischer-Frühholz, J. Juszcak, G. Erhardt, J. Buchberger, H. Klosterteyer, Isolation and rapid sequence characterization of two novel bovine β -Lactoglobulins I and J, *J. Protein Chem.* 15 (1996) 743–750.
- [35] K.M.G. Oliveira, V.L. Valente-Mesquita, M.M. Botelho, L. Sawyer, S.T. Ferreira, I. Polikarpov, Crystal structures of bovine β -lactoglobulin in the orthorhombic space group C2221: structural differences between genetic variants A and B and features of the Tanford transition, *Eur. J. Biochem.* 268 (2001) 477–483.

- [36] G.A. Manderson, L.K. Creamer, M.J. Hardman, Effect of heat treatment on the circular dichroism spectra of bovine beta-lactoglobulin A, B, and C, *J. Agric. Food Chem.* 47 (1999) 4557–4567.
- [37] D. Renard, J. Lefebvre, P. Robert, G. Llamas, E. Dufour, Structural investigation of β -lactoglobulin gelation in ethanol:water/solutions, *Int. J. Biol. Macromol.* 26 (1999) (350–44).
- [38] B. Jachimska, T. Jasiński, P. Warszyński, Z. Adamczyk, Conformations of poly (allylamine hydrochloride) in electrolyte solutions: experimental measurements and theoretical modeling, *Colloid Surface A* 355 (2010) 7–15.
- [39] K.P. Das, J.E. Kinsella, pH dependent emulsifying properties of β -lactoglobulin, *J. Dispers. Sci. Technol.* 10 (1989) 77–102.
- [40] L. Sawyer, G. Kontopidis, The core lipocalin, bovine beta-lactoglobulin, *Biochim. Biophys. Acta*, 1482 (200) 136–148.
- [41] T. Harnsilawat, R. Pongsawatmanit, D.J. McClements, Characterization of β -lactoglobulin-sodium alginate interactions in aqueous solutions: a calorimetry, light scattering, electrophoretic mobility and solubility study, *Food Hydrocoll.* 20 (2006) 577–585.
- [42] E.H.C. Bromley, M.R.H. Krebs, A.M. Donald, Aggregation across the length-scales in β -lactoglobulin, *Faraday Discuss.* 128 (2005) 13–27.
- [43] <http://protcalc.sourceforge.net>.
- [44] 'Protein interfaces, surfaces and assemblies' service PISA at the European Bioinformatics Institute. (http://www.ebi.ac.uk/pdbe/prot_int/pistart.html).
- [45] A. Schrems, A. Kibrom, S. Küpcü, U.B. Sleytr, B. Schuster, Bilayer lipid membrane formation on a chemically modified S-layer lattice, *Langmuir* 27 (2011) 3815–3821.
- [46] R. Zimmermann, U. Freudenberg, R. Schweiß, D. Küttner, C. Werner, Hydroxide and hydronium ion adsorption – a survey, *Curr. Opin. Colloid Interface Sci.* 15 (2010) 196–202.
- [47] P.J. Scales, F. Grieser, T.W. Healy, L.R. White, D.Y.C. Chan, Electrokinetics of the silica-solution interface: a flat plate streaming potential study, *Langmuir* 8 (1992) 965–974.
- [48] S.L. Walker, S. Bhattacharjee, E.M.V. Hoek, M. Elimelech, A novel asymmetric clamping cell for measuring streaming potential of flat surfaces, *Langmuir* 18 (2002) 2193–2198.
- [49] F. Höök, M. Rodahl, B. Kasemo, P. Brzezinski, Structural changes in hemoglobin during adsorption to solid surfaces: effects of pH, ionic strength, and ligand binding, *Proc. Natl. Acad. Sci. U. S. A.* 95 (1998) 12271–12276.
- [50] M.G.E.G. Bremer, J. Duval, W. Norde, J. Lyklema, Electrostatic interactions between immunoglobulin (IgG) molecules and a charged sorbent, *Colloid Surface A* 250 (2004) 29–42.
- [51] W. Norde, F. MacRitchie, G. Nowicka, J. Lyklema, Protein adsorption at solid-liquid interfaces: reversibility and conformation aspects, *J. Colloid Interface Sci.* 112 (1986) 447–456.
- [52] J.M. Lin, J.W. White, Denaturation resistance of β -lactoglobulin in monomolecular films at the air-water interface, *J. Phys. Chem. B* 113 (2009) 14513–14520.
- [53] J.J. Adams, B.F. Anderson, G.E. Norris, L.K. Creamer, G.B.J. Jameson, Structure of bovine β -lactoglobulin (variant A) at very low ionic strength, *J. Struct. Biol.* 154 (2006) 246–254.
- [54] J.D. Sherwood, Random sequential adsorption of lines and ellipses, *J. Phys. A* 23 (1990) 2827–2833.
- [55] W.L. DeLano, The PyMOL, Molecular Graphics System, 2002.
- [56] P.A.T. Martins, F. Gomes, W.L.C. Vaz, M.J. Moreno, Binding of phospholipids to β -lactoglobulin and their transfer to lipid bilayers, *BBA Acta-Biomembranes* 1778 (2008) 1308–1315.
- [57] B.L. Mellor, S. Khadka, D.D. Busath, B.A. Mazzeo, Influence of pKa shifts on the calculated dipole moments of proteins, *Protein J.* 30 (2011) 490–498.
- [58] S.S. Rogers, P. Venema, J.P.M. Van Der Ploeg, E. Van Der Linden, L.M.C. Sagis, A.M. Donald, Investigating the permanent electric dipole moment of β -lactoglobulin fibrils, using transient electric birefringence, *Biopolymers* 82 (2006) 241–252.
- [59] H. Pessen, J.M. Purcell Jr., H.M. Farrell, Proton relaxation rates of water in dilute solutions of β -lactoglobulin, Determination of cross relaxation and correlation with structural changes by the use of two genetic variants of a self-associating globular protein, *Biochim. Biophys. Acta Protein Struct. Mol. Enzymol.* 828 (1985) 1–12.